Hindawi
Journal of Electrical and Computer Engineering
Volume 2023, Article ID 5973076, 18 pages
https://doi.org/10.1155/2023/5973076

Research Article

Thermal Modeling of Photovoltaic Panel for Cell Temperature and Power Output Predictions under Outdoor Climatic Conditions of Jodhpur

Harish Kumar Khyani[1], **Jayashri Vajpai**[1], **Rajendra Karwa**[2], and **Mahendra Bhadu**[3]

[1]*Department of Electrical Engineering, M.B.M. University, Jodhpur, India*
[2]*Department of Mechanical Engineering, J.N.V. University, Jodhpur, India*
[3]*Department of Electrical Engineering, Bikaner Technical University, Bikaner, India*

Correspondence should be addressed to Mahendra Bhadu; mbhadu@alumni.iitd.ac.in

Received 8 August 2023; Revised 27 October 2023; Accepted 22 November 2023; Published 16 December 2023

Academic Editor: Mohamed Louzazni

The rise in the temperature severely affects photovoltaic cell efficiency and hence its power output. Moreover, it also causes the development of thermal stresses that may reduce their life span. Thus, there is a need for an accurate estimation of the cell's working temperature. In this paper, a detailed thermal model based on various heat transfer modes involved and their governing equations has been presented to estimate the cell temperature of a PV module using MATLAB software under different climatic and solar insolation conditions. In order to validate the presented model, an experimental setup has been built and operated under actual outdoor conditions of Jodhpur, a city in the Thar Desert of Rajasthan. For the peak summer month of June, the predicted glass cover outer surface temperature has been found to be within 0.2–4.5°C of experimentally measured values and the back sheet temperature is found to be within 0.5–5.5°C. The predicted and measured power outputs have been found to be within 0.85–1.2 W while the efficiency values are within 0.17–0.38%. For the early summer month of April, the variations are 0.13–4.1°C, 0.2–4.1°C, 0.44–1.65 W, and 0.1–0.5% for glass cover temperature, back sheet temperature, power output, and efficiency, respectively. Thus, the predictions of the developed thermal model have exhibited a good agreement with the experimental results. The maximum glass cover temperatures recorded were 60°C and 65.5°C when the ambient temperatures were 35°C and 42°C near the noon for the early summer and peak summer day experiments, respectively. The presented model can be used to generate a year-round cell temperature data for the known environmental data of a location, which can help in the selection or development of appropriate cooling technology at the planning stage of the installation of a solar PV plant.

1. Introduction

The conventional systems of electric power generation are associated with high carbon dioxide emissions with a threat of global warming. Thus, there is a dire need for greater use of solar photovoltaic (SPV) systems for sustainable development. As reported by the International Renewable Energy Agency (IRENA) [1], the global cumulative installed capacity of SPV systems was 1047 GW in 2022 and there is an increase of about 11 times over the last decade. International Energy Agency (IEA) [2] has predicted that the installed power capacity of SPV plants will surpass other energy technologies by 2027 and its share will be 22% of the cumulative power capacity as shown in Table 1.

As per the IEA report, India ranks fourth globally in terms of installed capacity of SPV plants. Among the states of India, Rajasthan has the highest installed capacity. Jodhpur region, which is located in the Thar Desert (a tropical desert) of Rajasthan, has the highest number of sunny days and high solar radiation intensity. Hence, this region is making rapid progress in the installation of solar PV generation systems. The installed SPV plants in the

Table 1: Share of cumulative power capacity by technology from 2010 to 2027 [2].

Technology	Share in different years (%)							
	2010	2015	2020	2021	2023	2024	2026	2027
Solar	0.8	3.5	9.4	10.9	14.7	16.5	20.2	22.2
Wind	3.5	6.5	9.4	10.1	11.4	12.1	13.7	14.4
Hydropower	19.8	18.9	16.9	16.6	15.7	15.2	14.5	14.1
Natural gas	26.7	25.2	23.3	22.6	21.4	20.8	19.7	19.1
Coal	31.2	30.6	27.5	26.7	24.7	23.8	21.9	20.9
Others	18	15.3	13.5	13.1	12.1	11.6	10	9.3

Jodhpur region have increased from 71 MW in 2011-12 to 3832 MW in 2021-22 (up to 31.8.21) [3], and this region has a huge potential for the expansion.

Electrical power output and efficiency are the main performance parameters of a solar PV system, which primarily depend on numerous influencing parameters. Several electrical models of varying complexity have been developed for the simulation-based study of the performance of solar PV systems [4]. However, the electrical model alone is not sufficient to provide the correct prediction of the electrical power output of the system because the thermal behaviour of the PV panel and the working temperature of the cell have a major impact on the output power and electrical efficiency of a PV cell.

The solar PV panels convert only a part of the incident solar radiation on the panel surface into electricity. A major portion of the incident solar radiation is absorbed by the panel which leads to an increase in the operating temperature of the cell. With respect to the values at standard test conditions (STCs), Masters [5] specifies that the open circuit voltage V_{oc} drops by about 0.37% for each degree Celsius increase in cell temperature, while the short circuit current I_{sc} increases by approximately 0.05% for crystalline silicon cells resulting in the decrease in the maximum power availability by about 0.5%/°C. Looking at this significant effect of the cell temperature on the performance of the cell, a thermal model is required to make a reasonably accurate estimation of the PV cell temperature for the given environmental and operating conditions. Several researchers have carried out studies on the thermal modeling of solar PV panels. A brief account of the major studies is being presented here.

Among the initial works, Fuentes [6] has reported the nominal operating cell temperature. In their independent research works, both Schott [7] and Jones and Underwood [8] have developed the linear thermal model of PV panels based on the energy balance. Knaup [9] has experimented with panel heat capacity and heat transfer for non-steady-state conditions. Mattei et al. [10] have developed two models based on the convection heat transfer coefficient related to the nominal operating cell temperature and energy balance, respectively, and found that the energy balance model provides better results. Skoplaki and Palyvos [11] and Dubey et al. [12] have presented a summary of expressions of the conversion efficiency and the output power with a focus on the thermal aspect. Kaplani and Kaplanis [13] carried out theoretical and experimental studies on the effect of wind velocity and wind incidence angle on PV module temperature. Armstrong and Hurley [14] studied the effect of rapidly changing solar radiation and wind speed to determine the thermal response time of the PV panel.

Kant et al. [15] have developed and validated a thermal model of polycrystalline solar PV panels through experimentation and examined the effect of change in temperature. Jaszczur et al. [16] have analyzed the temperature distribution in the PV panel under varying environmental conditions. Notton et al. [17] have proposed an electrical analogy-based finite difference model for a double-glass multicrystalline photovoltaic module, which was validated by utilizing the experimental data.

Tsai and Tsai [18] and Belhadj et al. [19] have presented an integrated electrical and thermal model for PV panels based on MATLAB/Simulink. Recently, Yaman and Arslan [20] have included transient conditions in their mathematical model to correctly determine the thermal and electrical parameters of a PV module. They have validated the model by comparing the simulation results with those from outdoor experiments carried out for multicrystalline silicon PV modules in summer conditions of Mersin, Turkey having minimum and maximum ambient temperatures of 22°C and 30°C, respectively, and wind velocity of 5–10 m/s. Under these conditions, the maximum cell temperature has been reported to be 50°C.

King et al. [21] and Duffie and Beckman [22] have presented thermal models with simplifying assumptions. The model of King et al. underestimated the cell temperature and the model of Duffie and Beckman overestimated it.

Aly et al. [23] employed a one-dimensional finite difference numerical technique to solve their thermal model for monofacial PV panels with polycrystalline silicon cells using the energy balance approach for different layers. The experimentally measured back sheet temperature of the PV panel was compared with the modeled back sheet temperature for different days of the year at Doha, which is a dry and an arid place. In Doha, the rainfall is very scanty and the months of June and July are the hottest months with maximum temperature averaging around 42°C.

Bevilacqua et al. [24] proposed a transient one-dimensional thermal model based on the energy balance method for photovoltaic modules consisting of polycrystalline silicon cells. The model was validated by comparing the predicted results using the method of finite differences and experimental data of the module back surface temperature and the electric power output in different seasons at Calabria (Italy) where the average maximum ambient temperature in summer is about 30°C.

Nicoletti et al. [25] presented an experimentally validated finite difference solution of a simple one-dimensional thermal model of a photovoltaic panel with polycrystalline cells for summer conditions of Calabria (Italy) having ambient temperature of 20–35°C and wind speed of 5–14 m/s (reaching occasionally up to 20 m/s). They recorded a maximum penal temperature of 62.1°C.

Khanam et al. [26] have numerically solved one-dimensional, quasisteady state experimentally validated thermal models of four different types of PV cells, namely, monocrystalline, polycrystalline, and thin films PV modules with opaque (Tedlar) and semitransparent (glass) back cover plates for four different climatic locations of India with the basic objective of prediction and comparison of their electrical efficiencies. They found that despite having a high potential for solar irradiation (higher radiation and greater number of sunny days) in Jodhpur, the annual electrical output was higher in Bangalore for all PV technologies. Khyani et al. [27] carried out outdoor experimentation at Jodhpur to measure the solar panel temperature. They observed that, in the summer months of April, May, and June 2021 with a maximum ambient temperature of 42.2°C in the month of May, the temperature of the solar panel on the front side reached up to 58.6°C, 65.7°C, and 63.9°C, respectively. These studies establish the dire need of finding cooling solutions for the PV panels for hot climatic conditions which prevail in areas such as the Jodhpur region.

Though an accurate estimation of cell temperature is essential, the operating temperature of the cells in the PV panels cannot be directly measured because the cells are inside the panels with layers of other materials surrounding them and, thus, are not accessible from outside [15]. Nishioka et al. [28] have attempted to measure it by fabricating the panel with internal temperature sensors directly inserted and attached to the cells. However, this is useful only for limited experimental purposes as it is associated with higher costs and lower versatility. Moreover, peeling off the back sheet is not advisable for inserting the sensors because the back sheet is used for the protection of PV cells from moisture and dust. In several cases of experimental research, the temperature of PV panels is measured by attaching temperature sensors to the back surface of the panels and in some cases infrared sensors and thermographic cameras have been used. Therefore, it can be concluded that the prevalent methods of determining cell temperature lack accuracy and have practical difficulties.

Jodhpur is located in the Thar Desert of western Rajasthan where the daytime summer temperature normally ranges from 40 to 45°C. In between, week-long spells of extremely high day temperatures of 46–48° have also been observed. The sky is generally clear and wind velocity seldom exceeds 2-3 m/s. It is notable that a high wind velocity is advantageous because it tends to cool the PV panel because of the increased convective heat transfer and the clear sky conditions help in greater heat rejection by radiation to the sky. It is also to be noted that the environmental conditions in Jodhpur are such that, in general, the changes are gradual, especially the solar radiation intensity and ambient temperature except when a sandstorm occurs in the summer, which are also not frequent since the last 3 decades.

None of the presented models available in the open literature are suitable for the very harsh summer conditions of western Rajasthan with low wind velocity, high ambient temperature, and intense solar radiation. Hence, the objective of the present work is to present a thermal model, which can fulfil the following requirements:

(i) It should be able to predict the cell temperature with reasonable accuracy even for extreme summer conditions and at the same time it should be simple enough for ease of application for the field engineers

(ii) It must consider all the heat transfer modes involved

(iii) It must be capable of predicting the cell temperature under different environmental and operating conditions because carrying out experiments covering all combinations of these parameters over a wide range is not a cost-effective and practical proposition

(iv) It must also be capable of predicting the power output and electrical efficiency of the PV panel with good accuracy

It is to be noted that the prediction of year-round data of the cell temperature for any location corresponding to the available environmental data at the planning stage can help in establishing the cooling requirement and also in the development of a suitable cooling technology.

2. Heat Transfer

The absorbed solar radiation in the cell raises its temperature above the ambient temperature. The heat from the cell is transmitted to the top and bottom faces of the PV panel and is rejected from there to the environment by convection and radiation. The equilibrium operating temperature of the cell can be determined from a thermal model, and subsequently the electrical power output corresponding to a particular set of solar radiation and other environmental parameters can be predicted. Figure 1 shows the multilayered construction of a solar PV panel [29]. The thermal properties of different layers of the PV panel are given in Table 2.

Some other properties required for thermal modeling are as follows:

(i) Transmissivity of glass, $\tau_g = 0.95$ [30]

(ii) Emissivity of glass, $\varepsilon_g = 0.88$ [31]

(iii) Transmissivity of the front encapsulant, $\tau_{E1} = 0.91$ [32]

(iv) Absorptivity of the PV cells, $\alpha = 0.9$ [33]

(v) Emissivity of back sheet, $\varepsilon_b = 0.91$ [34]

3. Energy Analysis of a Solar Photovoltaic Panel

The PV panel and the cell gain heat by absorbing a part of the incident solar radiation. The heated panel loses heat by convection and radiation to the environment. The heat from the cell flows through the various layers shown in

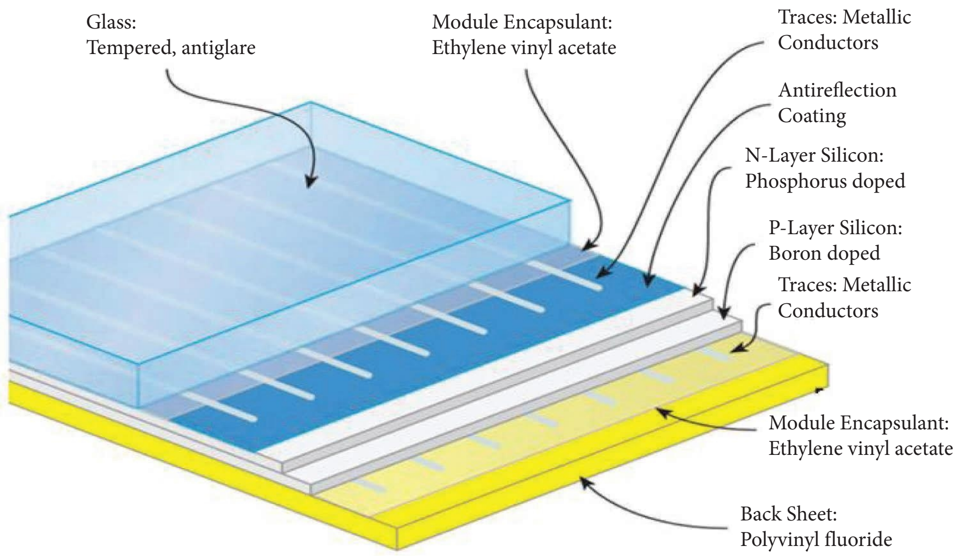

FIGURE 1: Basic construction of a solar PV panel [29].

Figure 1 above and below it by conduction and is finally lost from the panel's top and bottom surfaces by convection and radiation.

Figure 2 shows the energy balance of a solar PV panel. For the solar cell, the energy balance gives the following equation:

$$q_{\text{cell}} = [\text{IA}\,(\tau) - P]\alpha, \tag{1}$$

where P is the electric power output of the panel. For the incident solar radiation I over the unit panel area, IA (τ) reaches the cell surface after passing through the glass cover of transmissivity τ_g and front encapsulant $E1$ of transmissivity τ_{E1}, where τ is the effective transmissivity and is equal to $(\tau_g \times \tau_{E1})$.

The portion $[\text{IA}\,(1-\tau)]$ is partly reflected back and a part of it is absorbed in the glass cover and front encapsulant $E1$. The power output P depends on the efficiency η of the cell at its operating condition. Energy portion $[\text{IA}\,(\tau) - P]\ \alpha$ is absorbed in the cell, where α is the absorptivity of the cell, and it is converted into heat Qcell as given in equation (1). This absorbed heat causes a rise in the temperature of the cell. Since the absorptivity α is less than unity, a portion $(1-\alpha)\ [\text{IA}\,(\tau) - P]$ is reflected back from the cell surface. A part of this reflected radiation is also absorbed in the layers of the front encapsulant and glass cover. The efficiency of the cell is defined as

$$\eta = \frac{P}{\text{IA}}. \tag{2}$$

With the increasing ambient temperature, the stored heat in the multilayered structure of the module increases up to noon and this stored heat is released in the afternoon. The variations in the ambient temperature, wind velocity, and sky temperature affect the stored heat in the panel. Thus, basically, the panel experiences an unsteady state of operation. However, if these variations are gradual, a quasisteady state condition can be assumed when a short observation period of the order of 10 min is considered. For this assumption of quasisteady state condition, the variation in the stored heat is small. It is to be noted that ASHRAE Standard 93–77 [35] defines a quasisteady state with reference to the evaluation of the performance of solar collectors as the condition when the collector output changes gradually over a properly selected time period of 5–10 min. The standard permits the acceptance of such obtained results considering them to be of steady state.

The balance of energy is given by an equality in which the solar radiation that reaches the cell in the module will be equal to the sum of the electrical power that it delivers and the heat that it dissipates [36]. In the quasisteady state (treated as a steady state), the radiation absorbed in the cell as well as in the upper layers is rejected from the top and bottom surfaces of the panel, hence the energy balance can be written as

$$\text{IA}\,(\tau) \approx P + q_t + q_b, \tag{3}$$

where q_t is termed as the top loss and q_b is the back loss. Since a part of the incident solar radiation is also absorbed in the upper layers, the cell absorptivity α has been neglected in writing the energy balance equation. The modes of heat transfer involved are conduction, convection, and radiation.

The length and width of a PV panel are significantly larger than its thickness. Since the whole of the panel surface is subjected to a uniform flux of solar radiation, it can be expected that except near the edges, the variation in the temperature of the cell in the lengthwise and widthwise directions will be negligible. This gives a condition of one-dimensional conduction heat transfer across different layers in the direction of the thickness of the panel. The adoption of a one-dimensional (thicknesswise) variation of temperature approach can significantly simplify the thermal model. As mentioned earlier, Notton et al. [17] have proposed an electrical analogy-based one-dimensional finite difference

Table 2: Thermal properties of different layers of the PV panel.

S. no.	Layer (material)	Thickness δ (m)	Thermal conductivity k (W/(m·K))	Density ρ (kg/m^3)	Specific heat c_p (J/(kg K))	Conduction resistance[1] δ/kA (K/W)
1	Top cover (glass) [15]	3.2×10^{-3} (3.2 mm)	1.8	3000	500	1.8×10^{-3}
2	Antireflective coating (ARC) (silicon nitride) [14]	1.0×10^{-7} (1×10^{-4} mm)	32	2400	691	3.1×10^{-9}
3	Front and back encapsulant [15]	6.0×10^{-4} (0.6 mm)	0.35	960	2090	1.7×10^{-3}
4	PV cell (silicon) [15]	2.25×10^{-4} (0.225 mm) [14]	148	2330	677	1.5×10^{-6}
5	Back sheet (PVF) [15]	5.0×10^{-4} (0.5 mm)	0.2	1200	1250	2.5×10^{-3}

[1]Calculated values for $A = 1$.

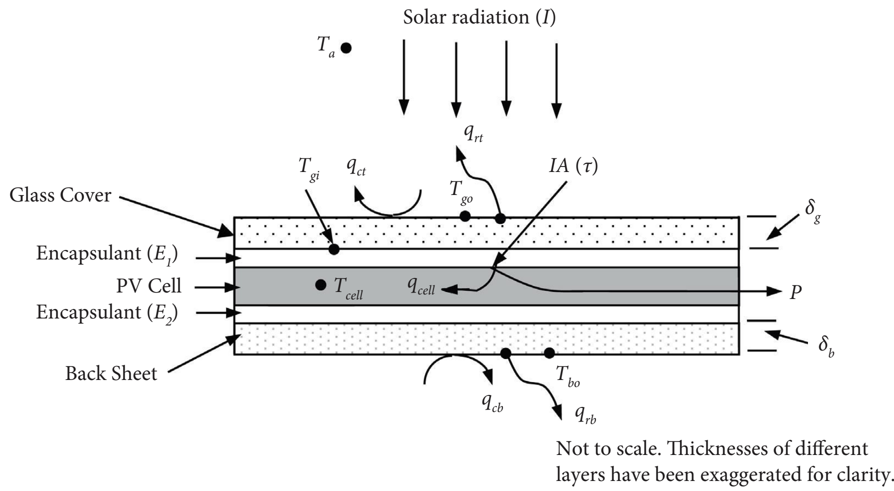

Figure 2: Energy balance on a solar PV panel.

model and Khanam et al. [26] in their numerical analysis of solar PV cells also considered one-dimensional heat conduction.

As discussed above, the absorbed heat raises the temperature of the cell above the ambient temperature and hence thermal gradients are established between different layers of the PV panel. The heat flows by conduction from the cell to the outer surface of the glass cover on the front side from where it is rejected by convection to the ambient air and by radiation to the sky. Similarly, heat flows by conduction to the outer surface of the back side from where it is rejected by convection to the ambient air and by radiation to the ground. Assuming the materials of different layers to be homogeneous and isotopic, the basic equation of conduction heat transfer as given by Fourier is

$$q_{\text{cond}} = kA\frac{\Delta T}{\delta} = \frac{\Delta T}{\delta/\text{kA}}, \tag{4}$$

where q_{cond} = heat flow rate by conduction, W, k = thermal conductivity of the layer, W/(m·K), A = area of the surface normal to the heat flow direction, m^2, ΔT = temperature difference across the layer, °C or K, δ = thickness of the layer, m, and δ/(kA) = thermal resistance to the conduction heat transfer.

The fundamental equation of combined convection and radiation heat transfer from a surface is as follows [31]:

$$q_{\text{conv}} + q_{\text{rad}} = A\left(h_c + h_r\right)\Delta T = \frac{\Delta T}{1/\left(h_c A\right)} + \frac{\Delta T}{1/\left(h_c A\right)}, \tag{5}$$

where h_c and h_r are the convective and radiative heat transfer coefficients, respectively, and $1/(h_c A)$ and $1/(h_r A)$ are the corresponding resistances.

Figure 3 shows the thermal network which helps in the heat transfer analysis for the estimation of top and back losses. As explained above in detail, since the thickness of the PV panel is very small in comparison to its length and width, the heat conduction that has been considered is one dimensional. The thickness of ARC is very small, and its conductivity is high. The resistance offered by this layer to conduction heat transfer is only 3.1×10^{-9} K/W, as given in Table 2. Hence, its resistance to conduction heat transfer has been neglected in the network presented in Figure 3. The effect of the frame has not been considered in the presented thermal model because it has a small surface area compared to the surface area of the panel and thus has a negligible

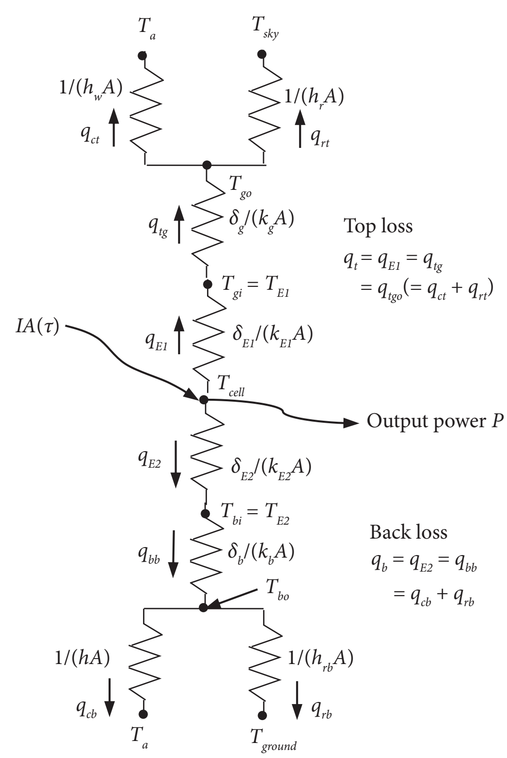

Figure 3: Thermal network for top and back losses of a solar PV panel.

effect on the temperature response of the PV panel [15]. The effect of metallic conductors has also been neglected.

Various temperatures indicated in the network are the equilibrium temperatures of (i) the cell T_{cell} (assumed to be uniform throughout its thickness because of the negligible conduction resistance of 1.5×10^{-6} K/W), (ii) glass side surface of encapsulant $(E_1)\,T_{E1}$, (iii) inner and outer layers of the glass T_{gi} and T_{go}, respectively, (iv) back sheet side surface of encapsulant $(E_2)\,T_{E2}$, and (v) the back sheet inner surface and outer surface T_{bi} and T_{bo}, respectively. The thermal contact resistance between different layers has been neglected in the presented analysis, which is in line with Aly et al. [23]. Hence, $T_{\text{gi}} = T_{E1}$ and $T_{bi} = T_{E2}$. In the network, T_a is the ambient temperature, T_{sky} is the sky temperature, and T_{ground} is the temperature of the ground facing the back sheet of the panel.

The thermal model presented in the next section deals with the various modes of heat transfer involved and presents the governing mathematical equations of these heat transfer modes and the power output equation.

4. Thermal Modeling of a Solar Photovoltaic Panel

A thermal model of the PV panel has been developed in this work. The simulation of the mathematical thermal model has been carried out using MATLAB. The major steps in the model-building strategy are as follows:

(1) Presentation of the mathematical equations of the various modes of heat transfer involved in the top and back losses
(2) Development of a computer program for the iterative solution of the set of mathematical equations to estimate the top and back losses, and the power output
(3) Estimation of the equilibrium temperature of the cell
(4) Validation of the mathematical model by comparing the predicted results with experimental data

4.1. Estimation of Top Loss q_t. Top loss is estimated by the iterative solution of the mathematical model for the same. The heat flows by conduction from the cell to the outer surface of the glass cover on the top and from where it is rejected by convection to the ambient air and by radiation to the sky.

Since the heat flows by conduction across the encapsulant E_1 of thickness δ_{E1} and thermal conductivity k_{E1} as depicted in Figures 2 and 3, the fundamental equation of conduction heat transfer, equation (4), gives

$$q_{E1} = \frac{T_{\text{cell}} - T_{E1}}{\delta_{E1}/(k_{E1}A)}, \tag{6}$$

where A is the area of the solar panel.

Similarly, the heat flows by conduction from the inner surface to the outer surface of the glass cover of thickness δ_g and thermal conductivity k_g, hence we have

$$q_{tg} = \frac{T_{\text{gi}} - T_{\text{go}}}{\delta_g/(k_g A)}. \tag{7}$$

From the outer surface of the glass cover at temperature T_{go}, the heat is lost by radiation to the sky at temperature T_{sky}. The convective heat transfer is due to the wind blowing over the surface of the panel. Hence, we have

$$q_{\text{tgo}} = q_{\text{rt}} + q_{\text{ct}}. \tag{8}$$

By using the fundamental equation of the combined convection and radiation heat transfer, equation (5), the heat loss is given by

$$\begin{aligned} q_{\text{tgo}} &= q_{\text{rt}} + q_{\text{ct}} \\ &= A\left[h_r\left(T_{\text{go}} - T_{\text{sky}}\right) + h_w\left(T_{\text{go}} - T_a\right)\right], \end{aligned} \tag{9}$$

where q_{rt} is the heat loss due to radiation to the sky from the top surface and q_{ct} is the heat loss by convection to the ambient air from the outer surface of the glass.

It is to be noted that the sky is considered as a blackbody at some fictitious temperature termed as sky temperature with which the outer surface of the glass cover exchanges heat by radiation. The sky temperature is a function of the relative humidity of air, atmospheric pollution including dust, the presence of clouds, and the ambient temperature, hence it is difficult to make a correct estimate of it. Investigators have estimated it using different correlations. A widely used equation for clear sky due to Swinbank [37] is $T_{\text{sky}} = 0.0552\ T_a^{1.5}$, which corresponds to the prevailing ambient temperature. In the Swinbank relation, both the temperatures are in Kelvin.

In equation (9), h_r is the radiation heat transfer coefficient for the top side. It is given by the following expression [31]:

$$h_r = \epsilon_g \sigma\left(T_{\text{go}}{}^2 + T_{\text{sky}}{}^2\right)\left(T_{\text{go}} + T_{\text{sky}}\right), \tag{10}$$

where σ is Stefan and Boltzmann constant and its value is $5.67\times10^{-8}\,\text{W}/(\text{m}^2\cdot\text{K}^4)$ and ε_g is the emissivity of the glass cover.

In equation (9), h_w is the wind heat transfer coefficient, which is a function of the wind velocity. It is determined by the following correlation given by McAdams [38]:

$$h_w = 5.62 + 3.91\,V_w \quad \text{for}\ V_w < 4.88\text{m/s}. \tag{11}$$

In the equilibrium, the top loss is calculated as

$$q_t = q_{E1} = q_{\text{tg}} = q_{\text{tgo}} = q_{\text{rt}} + q_{\text{ct}}. \tag{12}$$

4.1.1. Conduction Heat Transfer through the Upper Layers. Since from the cell to the glass outer surface, the conduction resistances of their layers are in series, we refer to the thermal network given in Figure 3, where $T_{\text{gi}} = T_{E1}$, and equations (6) and (7) give top loss as

$$q_{\text{cg}} = \frac{T_{\text{cell}} - T_{\text{go}}}{\delta_{E1}/k_{E1}A + \delta_g/k_g A}. \tag{13}$$

4.1.2. Convection and Radiation Heat Transfer from the Top Side. From equations (9) and (10), we have

$$q_{\text{tgo}} = h_w A\left(T_{\text{go}} - T_a\right) + \epsilon_g \sigma A\left({T_{\text{go}}}^4 - {T_{\text{sky}}}^4\right). \tag{14}$$

Hence, from equations (13) and (14), we get

$$\frac{T_{\text{cell}} - T_{go}}{\delta_{E1}/k_{E1}A + \delta_g/k_g A} = h_w A\left(T_{\text{go}} - T_a\right) + \epsilon_g \sigma A\left({T_{\text{go}}}^4 - {T_{\text{sky}}}^4\right). \tag{15}$$

The top loss is estimated by using the iterative solution of the governing equations and the main steps for the iteration are as follows:

(1) Initialize the cell temperature $T_{\text{cell}} = T_a + \Delta T$ for the known ambient temperature T_a

(2) Determine the wind heat transfer coefficient h_w from the measured wind velocity V_w

(3) Calculate the top loss q_t $(= q_{tgo})$ from equation (14) with a trial value $T_{\text{go}} = T_a + 1$ for the glass cover outer surface temperature

(4) With this first estimate of the top loss and after knowing the temperature of the cell, find the temperature of the outer surface of the glass cover from equation (13) and compare it with the trial value of T_{go}

(5) This calculated value of T_{go} is likely to be different from the trial value of T_{go}. Increase T_{go} by a small amount and recalculate the top loss q_t and T_{go} from equations (14) and (13), respectively. This new value of T_{go} is a trial value for the second iteration

(6) Repeat steps 4 and 5 and find a new T_{go}. This iteration will continue until the trial value of T_{go} and the calculated value of T_{go} are very close, say by 0.001°C

The flowchart for the iterative solution for the estimation of top loss is shown in Figure 4.

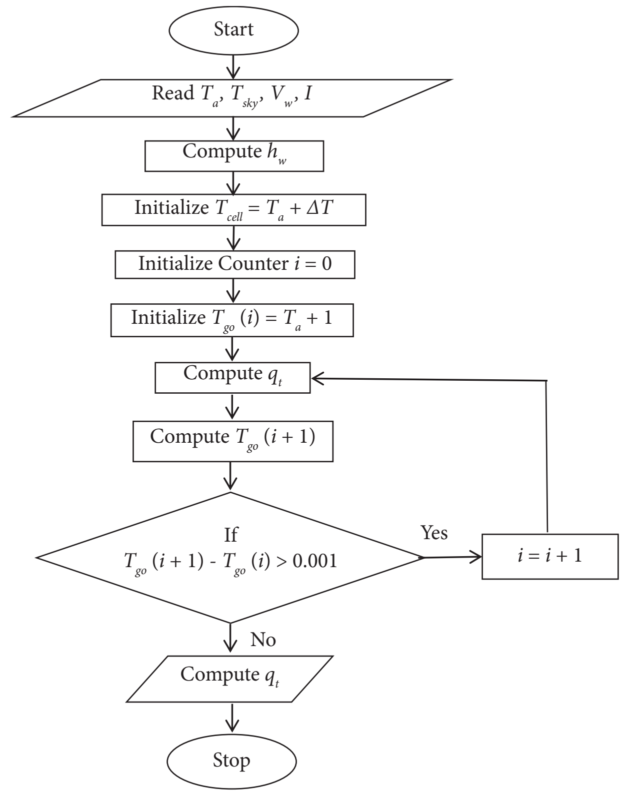

Figure 4: Flowchart for estimation of top loss.

From the outer surface of the back sheet at temperature T_{bo}, the heat is lost by radiation to the ground at temperature T_{ground}. The ground surface behaves as a black surface because the surface of the back sheet sees a large area on the ground [18]. On the back side of the panel, basically free convection condition is encountered [15] in contrast to the front of the panel which experiences a forced convection condition because of the blowing wind. Hence, the back loss using equation (5) is given by

$$q_b = q_{\text{rb}} + q_{\text{cb}} = A\left[h_{\text{rb}}\left(T_{\text{bo}} - T_{\text{ground}}\right) + h\left(T_{\text{bo}} - T_a\right)\right], \tag{18}$$

where T_{ground} is the temperature of the ground which is usually taken equal to the ambient temperature T_a [15], h is the convection heat transfer coefficient for the back side, and h_{rb} is the radiation heat transfer coefficient on the rear side. The radiation heat transfer coefficient is given by the following expression [31]:

$$h_{\text{rb}} = \epsilon_b \sigma\left({T_{\text{bo}}}^2 + {T_{\text{ground}}}^2\right)\left(T_{\text{bo}} + T_{\text{ground}}\right). \tag{19}$$

In the equilibrium,

$$\begin{aligned} q_b &= q_{\text{bb}} \\ &= q_{E2}. \end{aligned} \tag{20}$$

The free convection heat transfer coefficient h for the back side has been estimated from the mean Nusselt number correlation as follows:

4.2. Estimation of Back Loss q_b. Back loss is also estimated by using the iterative solution of the governing mathematical equations. The heat flows by conduction from the cell to the outer surface of the back sheet on the back side and the same is rejected by convection to the ambient air and by radiation to the ground.

Heat flows by conduction across the encapsulant E_2 of thickness δ_{E2} and thermal conductivity k_{E2}, hence we have

$$q_{E2} = \frac{T_{\text{cell}} - T_{E2}}{\delta_{E2}/\left(k_{E2}A\right)}. \tag{16}$$

Similarly, the heat flows by conduction from the inner to the outer surface of the back sheet of thickness δ_b and thermal conductivity k_b, and hence we have

$$q_{\text{bb}} = \frac{T_{E2} - T_{\text{bo}}}{\delta_b/\left(k_b A\right)}. \tag{17}$$

$$h = \frac{\mathrm{Nu}.k}{L}, \tag{21}$$

where Nu = Nusselt number, k = thermal conductivity of air at the mean film temperature $T_m = (T_{\mathrm{bo}} + T_a)/2$, and L = length of back sheet.

Nusselt number has been determined from the following relation by Churchill and Chu (in reference [31]) as follows:

$$\mathrm{Nu} = \left\{ 0.825 + \frac{0.387\,\mathrm{Ra}^{1/6}}{\left[1 + (0.492/\,\mathrm{Pr})^{9/16}\right]^{8/27}} \right\}^2 \text{ for } 10^{-1} \le Ra \le 10^{12}, \tag{22}$$

where Ra is the Rayleigh number for an inclined surface. It is given by the following relation:

$$\mathrm{Ra} = \frac{\rho^2 \beta g \sin\theta \left(T_{bo} - T_a\right) L^3}{\mu^2}\,\mathrm{Pr}, \tag{23}$$

where $\beta = (1/T_m)$ = coefficient of cubical expansion, $T_m = (T_{\mathrm{bo}} + T_a)/2$ = mean film temperature, K, ρ = density of air at mean film temperature, θ = angle of inclination of the back sheet with the vertical, and Pr = Prandtl number. It is given by the following relation as follows:

$$\mathrm{Pr} = \frac{\mu . c_p}{k}, \tag{24}$$

where μ is the viscosity of air and c_p is the specific heat of air at the mean film temperature.

4.2.1. Thermophysical Properties of Air. All thermophysical properties of the air (k, ρ, μ, and c_p) have been taken at the corresponding mean film temperature T_m by using the following relations [31]:

$$k = 0.0257\left(T_m/293\right)^{0.86}, \tag{25a}$$

$$\rho = 1.204\left(293/T_m\right), \tag{25b}$$

$$\mu = 1.81 \times 10^{-5}\left(T_m/293\right)^{0.735}, \tag{25c}$$

$$c_p = 1006\left(T_m/293\right)^{0.0155}, \tag{25d}$$

where all temperatures are in *K*.

4.2.2. Conduction Heat Transfer through Back Side Layers. The conduction resistances of the layers are in series hence, from equations (16) and (17), the top loss is calculated as

$$q_{cb} = \frac{T_{\mathrm{cell}} - T_{\mathrm{bo}}}{\delta_{E2}/k_{E2}A + \delta_b/k_b A}. \tag{26}$$

4.2.3. Convection and Radiation Heat Transfer from the Back Side. From equations (18) and (19), we have

$$q_b = \mathrm{hA}\left(T_{\mathrm{bo}} - T_a\right) + \epsilon_b \sigma A\left({T_{\mathrm{bo}}}^4 - {T_{\mathrm{ground}}}^4\right). \tag{27}$$

From equations (26) and (27), we get

$$\frac{T_{\mathrm{cell}} - T_{\mathrm{bo}}}{\delta_{E2}/k_{E2}A + \delta_b/k_b A} = \mathrm{hA}\left(T_{\mathrm{bo}} - T_a\right) + \epsilon_b \sigma A\left({T_{\mathrm{bo}}}^4 - {T_{\mathrm{ground}}}^4\right). \tag{28}$$

In order to solve equation (28), it is required to estimate the value of h and T_{bo}, hence an iterative process has been used. The major steps for the estimation of h and T_{bo} and hence the back losses are as follows:

(1) We start with cell temperature T_{cell} initialized in step 1 of the iterative process for top loss estimation and a trial value of $T_{\mathrm{bo}} = (T_{\mathrm{cell}} + T_a)/2$. We estimate T_m and h and then calculate q_b $(= q_{cb})$ from equation (27) and T_{bo} from equation (26). This calculated value of T_{bo} is likely to be different from the trial value of T_{bo}.

(2) We consider a new value of T_{bo} with a small change from the trial value of T_{bo} in step 1, which may be termed as T_{bo} (1). Again, we estimate T_m and h and then calculate q_b and T_{bo} from equations (27) and (26), respectively.

(3) If the calculated value of T_{bo} in step 2 differs by more than 0.001°C from T_{bo} (1), then we consider a new value of T_{bo} with a small change from T_{bo} (1), say T_{bo} (2). This process is continued till the two successive values of T_{bo} do not differ by more than 0.001°C.

The flowchart for the iterative solution for the estimation of back loss is shown in Figure 5.

4.3. Estimation of Power Output P. The efficiency of a PV cell is given by the following fundamental expression as a function of operating cell temperature T_{cell} [39]:

$$\eta = \eta_{\mathrm{ref}}\left[1 - \beta_{\mathrm{ref}}\left(T_{\mathrm{cell}} - T_{\mathrm{ref}}\right)\right], \tag{29}$$

where η_{ref} = efficiency of the module at STC = 13.2%, T_{ref} = reference temperature of STC = 25°C, and β_{ref} = temperature coefficient = 0.5% per °C

Knowing the efficiency, the power output is calculated from

$$P = \eta\,(\mathrm{IA}). \tag{30}$$

Since equation (3) of the energy balance must be satisfied, the LHS of this equation must be equal to or very close to the RHS, say LHS-RHS ≤1 W. If this condition is not satisfied, the cell temperature T_{cell} is increased by a small amount from its initial value of $T_{\mathrm{cell}} = T_a + \Delta T$ as mentioned in step 1 of the iterative process for top loss estimation. Then, new estimations of top loss q_t, back loss q_b, and power output P are made. This process is continued till the energy balance condition defined by equation (3) is satisfied.

To carry out the iterative process outlined above for the estimations of top and back losses, and power output, two functions have been created separately in MATLAB to estimate the top and back losses. The main iterative MATLAB program has been written to call these functions along with the initial value of T_{cell} and the measured values of the environmental data for the estimation of output power and

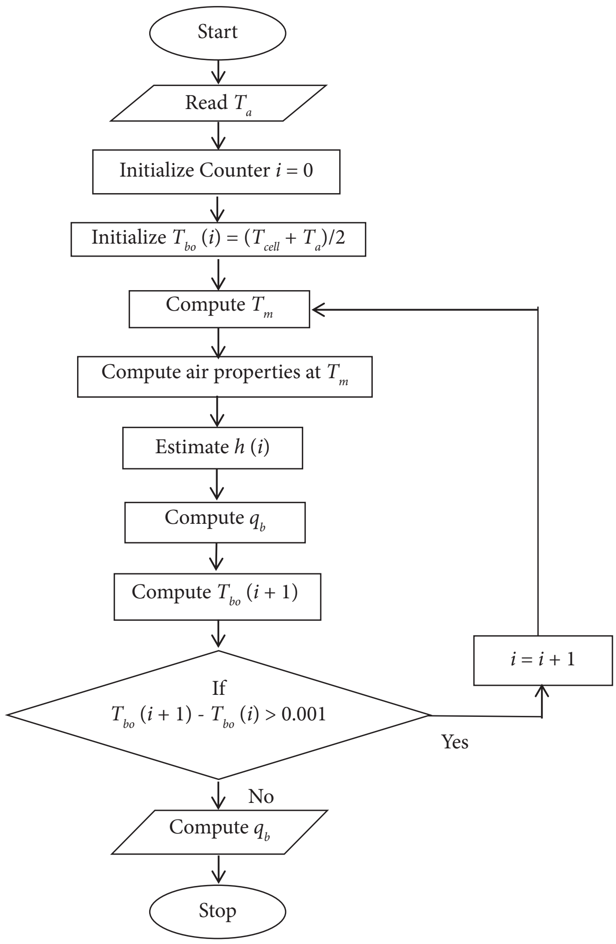

Figure 5: Flowchart for the estimation of back loss.

checking the energy balance. If the energy balance condition is not satisfied, the initial value of cell temperature is increased by a small amount and the process of estimations of top loss, back loss, and power output is repeated till the condition of satisfaction of the energy balance equation is achieved.

5. Experimental Validation of the Thermal Model

In order to validate the thermal model, an experimental test facility has been set up on the rooftop of the Electrical Engineering Department of M.B.M. University, Jodhpur (India).

The setup consists of an equipment for the measurement of various environmental parameters, namely, solar radiation intensity I, ambient temperature T_a, wind velocity V_w, and sky temperature T_{sky}. Other parameters measured are the PV panel's front glass cover and back sheet surface temperatures T_{go} and T_b, respectively, and output voltage and current. The validation is based on the accuracy of the prediction of the average temperatures of the top and back surfaces of the PV panel, power output, and efficiency with respect to their experimentally measured values.

The details of the experimental setup are given in the next section.

5.1. Experimental Setup. The details of the apparatus used for the experiment are given in Table 3. It consists of a digital solar radiation recorder, an automatic wind monitor, a contactless infrared thermometer, an ambient temperature measurement unit (Stevenson screen), and a programmable DC load. The solar radiation recorder and wind monitor were fixed at the height of the PV panel. The schematic diagram of the experimental setup and its photograph are given in Figures 6 and 7, respectively.

The manufacturer's data for the REIL201129019 solar PV panel are given in Table 4. Since the yearly electrical energy output of a PV panel is maximum at an inclination of the latitude of the location, the panel was installed facing south (with no buildings or trees in view of the panel face) at an inclination of 26° with a horizontal inclination for 26.3° N latitude of Jodhpur.

5.2. Experimental Procedure. The solar radiation I at the plane of the panel was measured by using a digital solar radiation recorder, the wind velocity V_w was measured with the help of an automatic wind monitor, a temperature measurement unit (Stevenson screen) was used for the measurement of ambient temperature, and the front and back surface temperatures of the PV panel and sky temperature were measured by means of a contactless infrared (IR) thermometer. The sky temperature has been taken as an average of the readings recorded by pointing the IR thermometer towards the sky at various angles from the zenith as suggested in reference [40]. The method of estimating the sky temperature adopted in the present study is also the same as described in reference [41]. The output voltage and current of the PV panels were measured with the help of a digital multimeter after connecting the programmable DC load operated in the constant resistance mode.

The day-long experiments have been conducted with PV panels installed on the rooftop as mentioned earlier, i.e., under real operating conditions. All readings as described above were recorded at an interval of 30 min. Early summer and peak summer days with nearly clear sky conditions have been selected for the results reported in the next section.

Experimentally, surface temperatures of the glass cover and the back plate were directly measured with uncertainty in the measurement of ±2°C. The power output of the panel has been calculated from the measured voltage and current values. The efficiency of the cell has been calculated from equation (2).

From the analysis of the uncertainties in the measurements, the uncertainties in the calculated values of various parameters using the method of Kline and McClintock [42] are as follows:

$$\text{Power} = \pm 0.94\% \text{ (odds of 20–1)}$$
$$\text{Efficiency} = \pm 4.1\% \text{ (odds of 20–1)}$$

The significant contributor to the uncertainty in the efficiency is the uncertainty in solar radiation measurement as depicted in Table 3.

Table 3: Details of the apparatus used for the experiment.

Name	Make	Model	Rating/range	Accuracy
Solar panel (as detailed in Table 2)	REIL	201129019	75 W	±3%
Digital solar radiation recorder	Virtual	SRR-VH-SR-D	0–2000 W/m^2	±4%
Automatic wind monitor	Virtual	WM-VH-SS-D	For wind speed 0.5–6.7 m/s	Accuracy better than 0.5 m/s
Contactless infrared thermometer	Smart sensors	AR320	−32°C–320°C, emissivity = 0.95 (preset)	±2°C/±2%
Programmable DC load	Sensetechno Solutions	STDCPL01	80 V, 300 W, 15 A, 0–40 Ω	±1%
Ambient temperature measurement unit with mercury thermometer (Stevenson screen)	JK	72074	0–110°C	±1.5°C
Digital multimeter	Metravi	451	0–1000 V/0–20 A/0–2000 MΩ	±0.5%/±0.8%/±0.8%

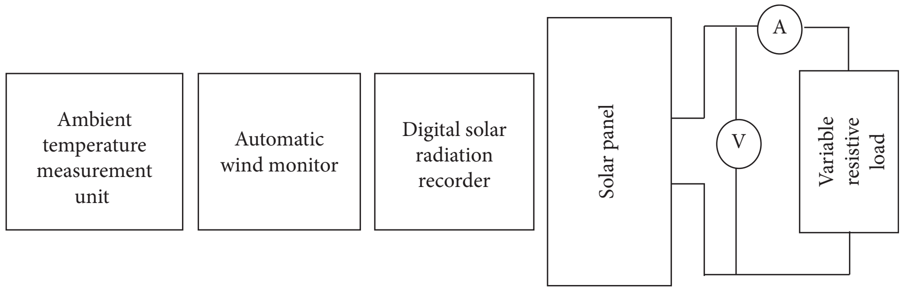

Figure 6: Schematic diagram of the experimental setup.

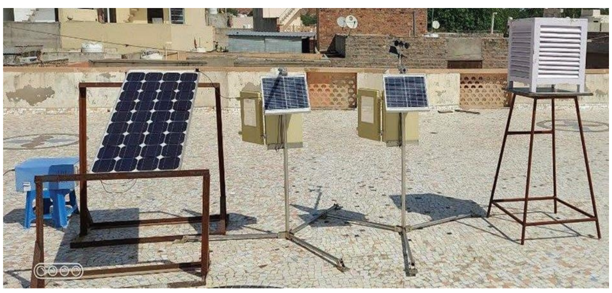

Figure 7: Photograph of the experimental setup.

Table 4: Parametric specifications of REIL201129019 monocrystalline silicon PV panel.

Characteristic parameters	Specifications
Maximum power, P_{max} (watts)	75 W_p
Voltage at maximum power point, V_{max} (volts)	17.0
Current at maximum power point, I_{max} (amps)	4.6
Open circuit voltage, V_{oc} (volts)	21.5
Short circuit current, I_{sc} (amps)	5.3
Maximum system voltage	600 V DC
Number of cells/panel	36 (4×9)
Electrical parameter tolerance	±3%
Size of the panel (mm)	$1200 \times 535 \times 33$
Area (m^2)	0.642
Weight (kg)	7.5

Karwa et al. [43] have presented sensitivity analysis for their theoretical study by using a mathematical model. The sensitivity analysis for the present study shows that, typically at $T_a = 40°C$, $V_w = 0.75$ m/s, $I = 725$ W/m^2, and $T_{sky} = 20°C$, +1°C change in the ambient temperature affects the cell temperature T_{cell} prediction by +0.7°C and the power output prediction by −0.4%. A change of +0.5 m/s in wind velocity V_w affected T_{cell} prediction by −1.5°C and power output prediction by +0.9%. These values are about +0.4°C and +1.1%, respectively, for a +10 W/m^2 change in solar radiation, while a +5°C change in the sky temperature affected these values by +1.0°C and −0.6%, respectively.

5.3. Validation of the Thermal Model. In order to validate the thermal model, the experiments have been conducted on April 23, 2023, and June 25, 2022, which are early summer and peak summer days, respectively. The days of experiments had nearly clear sky conditions. The comparison of the experimental results has been made with the predicted values from the model. It is to be mentioned that the measured value of sky temperature has been used in the mathematical model for its validation.

The recorded values of the environmental parameters are presented in parts (a) and (b), while experimental data and predicted values of temperatures of the penal front and back surfaces, and power output are presented in parts (c) and (d) of the plots of Figures 8 and 9 for April 23, 2023, and June 25, 2022, respectively.

In Figure 8, it can be seen that the predicted glass cover outer surface temperature values are within 0.13–4.1°C of experimentally measured values, while the predicted back sheet temperature values are within 1.2–4.1°C of the experimentally recorded values. The predicted and measured power output values are within 0.44–1.65 W. The RMSE values for top and bottom surface temperatures are found to be of 4.11°C and 2.03°C, respectively. For power output, RMSE is found to be of 1.19 W.

Figure 9, which refers to the peak summer day of June 2022, shows that the presented thermal model can predict the front glass cover outer surface temperature within 0.2–4.5°C of the experimental values and the predicted back sheet temperature values are within 0.5–5.5°C of the corresponding experimentally recorded values. The predicted and measured power output values can be seen to be within 0.85–1.2 W. The RMSE values for the top and bottom surface temperatures are found to be of 2.35°C and 3.57°C, respectively. For the power output, RSME is 1.09 W.

The predicted values of cell temperature have been used in equation (29) of the model to determine the power output of the panel as explained in Section 4. Experimentally, the power output is calculated from the observed values of voltage across and current through the load in the electrical circuit of the experimental setup.

The predicted and experimental electrical efficiencies of the PV panel are plotted versus the time of the day in Figure 10. The predicted and measured efficiencies are within 0.08–0.52% with a RMSE value of 0.27% for April 23, 2023, while the predicted and measured efficiency values for June 25, 2022, are within 0.17–0.38% with a RMSE value of 0.27%.

The variation of the efficiency with time of the day for both days of the experimentation is similar to those reported by Khanam et al. [26] and Elminshawy et al. [44]. As seen in Figures 8(d) and 9(d), the power output follows the trend of variation of the solar radiation intensity. The power output

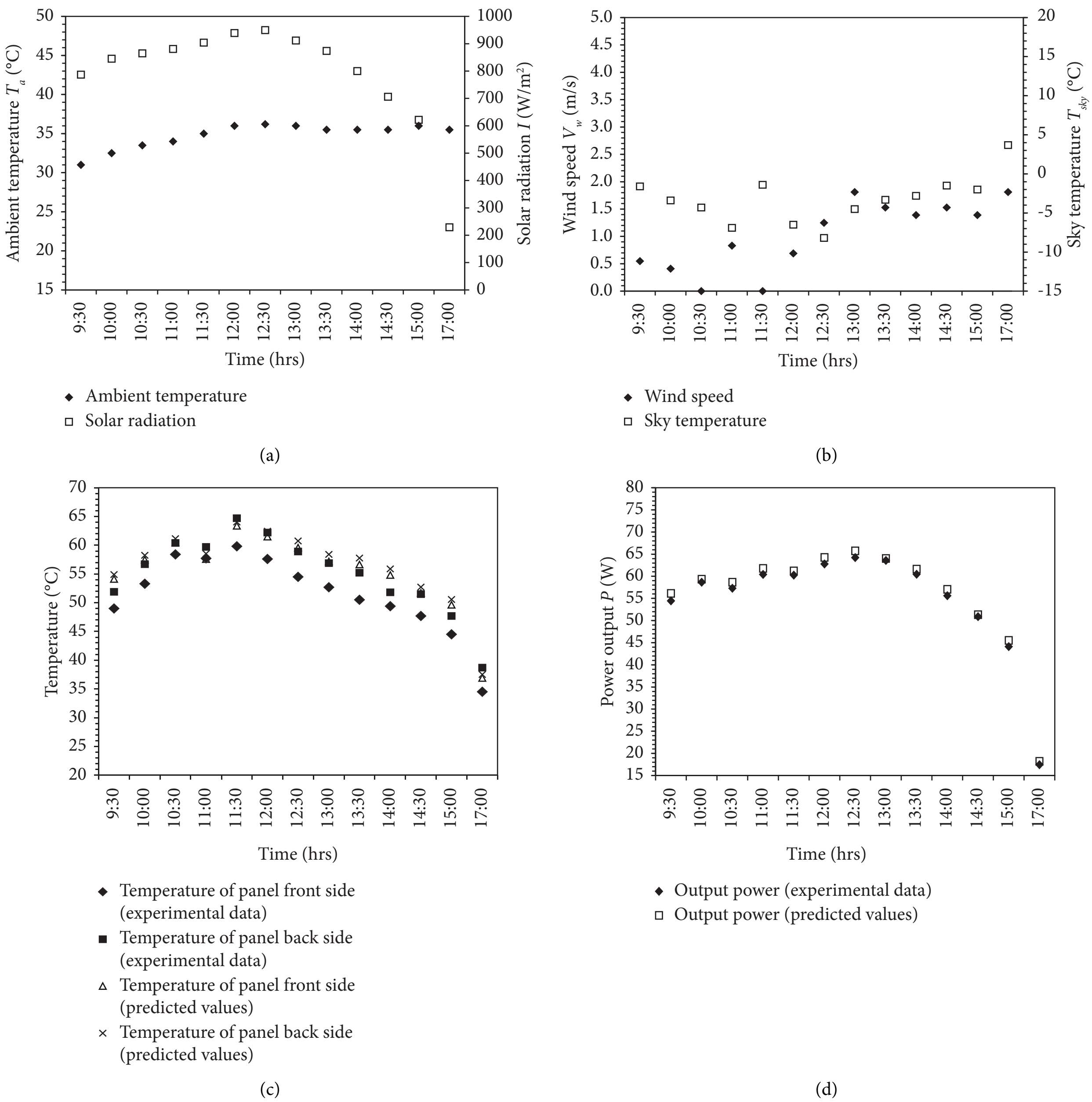

FIGURE 8: (a, b) Environmental parameters T_a, I, V_w, and T_{sky}, (c) panel surface temperatures, and (d) power output (predicted and experimental) versus time of the day (April 23, 2023).

increases from morning hours to afternoon with the increase in the solar radiation intensity and then it is seen to decrease during the afternoon. From Figures 8(c) and 9(c), it can be seen that the PV penal temperatures increase with the time of the day up to the afternoon and then decrease, and, thus, this trend nearly follows the variation of the solar radiation intensity. It is to be noted that the ambient temperatures also affect the panel temperature, which increases in the forenoon period with the increase in the solar radiation but the decrease in the afternoon temperature does not follow the trend of solar radiation intensity and remains high. From the plots of efficiency in Figure 10, it can be seen that the efficiency variation shows a trend which is opposite to the trend of variation of the solar radiation intensity. Khanam et al. have explained the reason for this trend. The increase in the cell temperature excites the electrons which enhances the collisions between them and thereby increases the resistance, and hence the efficiency of the PV cell decreases in the middle hours.

The predicted and experimental values of various parameters discussed above can be considered to be in close agreement and practically acceptable. Hence, it can be inferred that the thermal model is validated to an acceptable degree of accuracy and the model can be used to predict the cell temperature as well, which is not possible to measure directly.

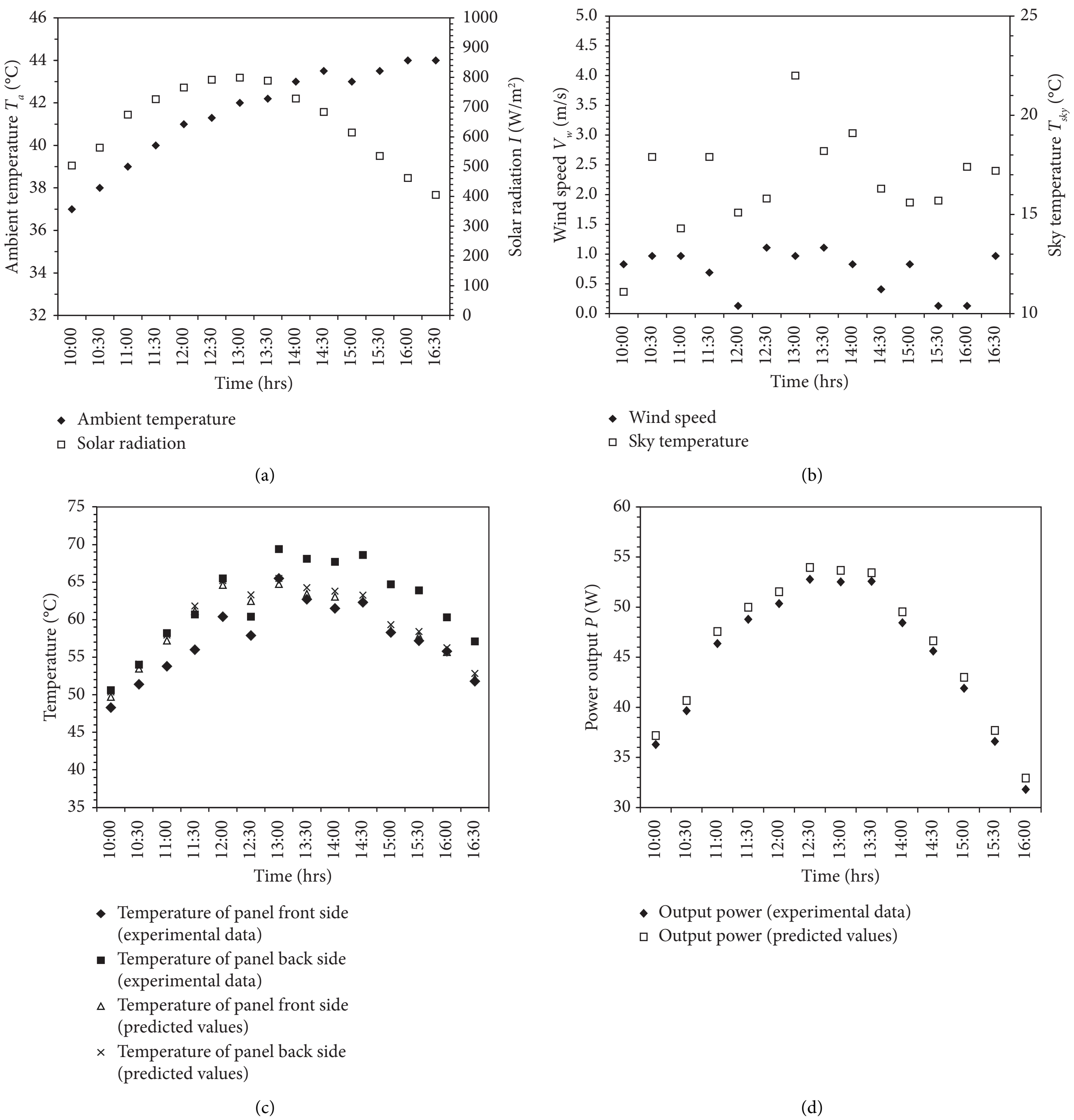

FIGURE 9: (a, b) Environmental parameters T_a, I, V_w, and T_{sky}, (c) panel surface temperatures, and (d) power output (predicted and experimental) versus time of the day (June 25, 2022).

It is to be noted that the observed differences in the predicted and measured results are due to the fact that there are uncertainties in the estimates of sky temperature and wind heat transfer coefficient. The uncertainties in these parameters have been discussed in significant detail in reference [41]. Furthermore, it is mentioned that there is also an uncertainty in the estimate of the convective heat transfer coefficient on the back surface of the panel.

The fulfilment of the condition of one-dimensional conduction heat transfer mentioned earlier has been confirmed experimentally. The size of the PV panel used in the present study is 1200 mm in length, 535 mm in width, and 33 mm in thickness Along the length of the panel, the glass and back surface temperatures were measured at nine approximately equally spaced locations to find their average temperatures. The temperature at these locations was found to be within 2.5°C. In the spanwise direction, the temperature was measured at equally spaced 7 locations at the midheight of the panel. In the spanwise direction, the variation in the measured temperature was found to be less than 1.5°C. Since the variation of the temperature per unit distance is negligible in lengthwise and widthwise directions, so looking at the length and width of the panel, the assumption of one-dimensional conductive heat transfer

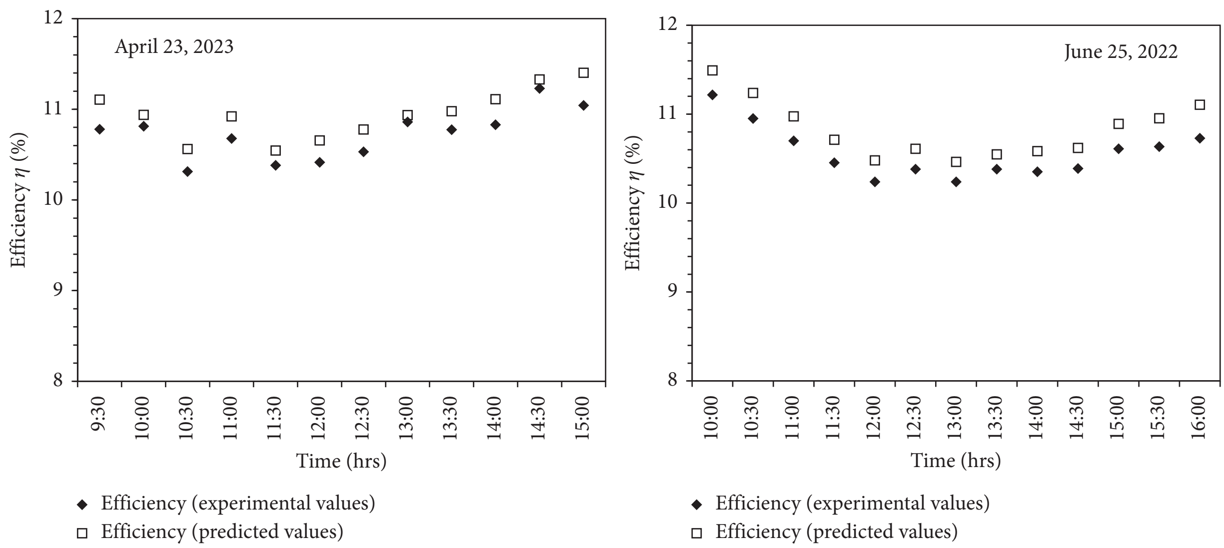

Figure 10: Predicted and experimental efficiency values versus time of the day.

across the thickness of the panel is justified. It is to be mentioned that the extreme locations for temperature measurements were kept about 50 mm away from the frame of the panel. This approach is also in line with Kant et al. [15] who did not consider the effect of the frame of the panel extending the logic that the frame has a low surface area with respect to the panel area and, thus, has a negligible effect on the temperature response of the PV panels. Aly et al. [23] have ignored the thermal conductance towards the frame in the analysis of their thermal model.

The cell temperature for the environmental condition of June experiment day has been found to vary from about 51°C at 10 am to a maximum of about 66.5°C at the noon and 53°C at 4:30 pm when the ambient temperature was 37–44°C giving the difference between the cell and ambient temperatures of about 14°C at 10 am, 25°C at noon, and 9°C at 4:30 pm. At noon, the experimental value of the glass cover temperature was found to be 65.5°C when the ambient temperature was 42°C. For the day of the experiment in April, the maximum cell temperature was found to be about 60°C when the ambient temperature was 35°C. The observed temperature difference between the glass cover and back sheet temperatures is found to be of the order of magnitude in line with Santiago et al. [36] who reported that the cell junction temperatures were typically 1–3°C higher than the temperature measured on the module's rear surface depending on the module construction and material. It is also to be noted that the temperature of the back sheet of the panel is always higher than the temperature of the glass cover surface.

Since the operating conditions vary throughout the year, month, and even in a day, and they also depend on the location, so it is not cost-effective and practically possible to carry out experiments covering all combinations of these parameters over a wide range. The presented model can be used to generate a year-round data of the cell temperature, power output, and efficiency for any location for known values of ambient temperature, solar insolation, and wind velocity. This information can be utilized to select or develop appropriate cooling technology at the planning stage of the solar PV plant, which can significantly enhance the performance of the solar PV system. This aspect has a special significance in the tropics where the operating temperature of the PV cell is very high because of the high day time temperatures such as in the Thar Desert of Rajasthan where large solar PV generation systems are being installed. It has been mentioned earlier that the back sheet temperature is higher than the glass cover temperature, hence the back sheet can be targeted for the cooling of the panel without interfering with the incoming solar radiation on the front face.

6. Conclusions

A thermal model has been presented in this study to predict the cell temperature, power output, and efficiency under outdoor operating conditions. The presented model is based on the mathematical equations of various heat transfer modes involved and energy balance along with the equation for the prediction of the electrical power output.

The validation of the presented model has been carried out with experimental data. The predicted values of glass cover outer surface temperature, back sheet temperature, power output, and efficiency by the model are found to be within 0.2–4.5°C, 0.5–5.5°C, 0.85–1.2 W, and 0.17–0.38%, respectively, of the experimentally measured values for the peak summer month of June when the ambient temperature recorded was 37–44°C. The maximum glass cover temperatures recorded were 60°C and 65.5°C when the ambient temperatures were 35°C and 42°C near the noon for the early summer and peak summer day experiments, respectively. For the early summer month of April, these values were found to be of 0.13–4.1°C, 0.2–4.1°C, 0.44–1.65 W, and 0.1–0.5% for the glass cover outer surface temperature, back sheet temperature, power output, and efficiency, respectively. Thus, the predictions of the thermal model have exhibited a good agreement with the experimental results.

The presented model can be employed to generate a year-round cell temperature data for the available environmental data. This can help in the selection or development of an appropriate cooling technology at the planning stage of installation of a solar PV generation facility especially for the commercial-level solar PV plants.

6.1. Recommendations for Future Work. The study in this paper has been carried out on a single PV module of 1200 mm × 535 mm area. In actual field applications, the modules are arranged in series and parallel to form arrays of different areas depending on the power output requirements. This study may be extended to the arrays because the effect of the wind on larger areas of the arrays is significantly different. For the flow of any fluid over a flat surface (here, the fluid is air in the form of wind), the thermal boundary layer development and its characteristics, and the flow Reynolds number change with distance from the leading edge of the array surface in the direction of the flow. This causes significant changes in the value of the wind heat transfer coefficient for the same wind velocity, which is a definite variation from the McAdam's relation presented in this study. It is to be noted that the wind velocity has a prominent effect on the cooling of a PV panel. On the other hand, the temperature of the blowing wind would increase as it moves along the surface of the array and its cooling effect reduces. Furthermore, in the city areas, the rooftop arrays experience different wind patterns than in the fields and the area of the arrays is also much smaller.

In the city areas, the sky temperature is much higher than predicted from Swinbank relation for clear sky due to the environmental pollution. The relative humidity also affects the sky temperature. The effects of these factors are needed to be investigated.

The information generated using the thermal model about the working temperature of the cell under different environmental conditions can help in the selection/development of an appropriate cooling technology at the planning stage of solar PV installations. The cooling of the solar PV panel is an area of great research interest. It has special significance especially for the arid regions such as that of the western Rajasthan where the water availability is very poor and the ambient temperatures are high.

Nomenclature

A: Area of the solar panel, m^2
c_p: Specific heat of air, J/(kg·K)
h: Convection heat transfer coefficient for back side, W/(m^2·K)
h_r: Radiation heat transfer coefficient for front as well back side, W/(m^2·K)
h_w: Wind heat transfer coefficient, W/(m^2·K)
I: Solar radiation, W/m^2
k: Thermal conductivity of air, W/(m·K)
k_b: Thermal conductivity of the back sheet, W/(m·K)
k_{E1}: Thermal conductivity of the front encapsulant, W/(m·K)
k_{E2}: Thermal conductivity of the back encapsulant, W/(m·K)
k_g: Thermal conductivity of the top glass cover, W/(m·K)
L: Length of the PV Panel, m
Nu: Nusselt number
P: Power output of the PV Panel, W
Pr: Prandtl number
q_b: Total heat loss from the back side, W
q_{cb}: Heat loss due to convection to the ambient air from the back side, W
q_{cell}: Heat absorbed in the solar cell, W
q_{ct}: Heat loss due to convection to the ambient air from the outer side of the glass cover, W
q_{rb}: Heat loss due to radiation to the ground from the back side, W
q_{rt}: Heat loss due to radiation to the sky from the outer side of the glass cover, W
q_t: Total heat loss from the top side, W
Ra: Rayleigh number
T_a: Ambient temperature, K
T_{bo}: Temperature of the outer surface of the back sheet, K
T_{cell}: Temperature of the solar cell, K
T_{gi}: Temperature of the inner surface of the glass cover, K
T_{go}: Temperature of the outer surface of the glass cover, K
T_{ground}: Temperature of the ground, K
T_m: Mean air film temperature, K
T_{sky}: Sky temperature, K
V_w: Wind velocity, m/s

Greek Symbols

α: Absorptivity of the PV cells
β: Coefficient of cubical expansion, 1/K
δ_b: Thickness of the back sheet, mm
δ_{E1}: Thickness of the front encapsulant, mm
δ_{E2}: Thickness of the back encapsulant, mm
δ_g: Thickness of the glass cover, mm
θ: Angle of inclination of the PV panel with the vertical, degree
ε_g: Emissivity of glass
ε_b: Emissivity of the back sheet
η: Efficiency of the PV cell
μ: Viscosity of air, kg/(m·s)
ρ: Density of air, kg/m^3
σ: Stefan and Boltzmann constant = 5.67 × 10−8 W/(m^2·K^4)
τ: Transmissivity of glass
τ_α: Transmittance-absorptance product
τ_{E1}: Transmissivity of the front encapsulant.

Data Availability

The author elects to not share data, as this publication is an outcome of ongoing research work for Ph.D. thesis.

Conflicts of Interest

The authors declare that they have no conflicts of interest.

References

[1] irena, "Renewable energy statistics," 2023, https://www.irena.org/Publications/2023/Mar/Renewable-capacity-statistics-2023.

[2] iea, "Renewables," 2022, https://www.iea.org/reports/renewables-2022/executive-summary.

[3] rajasthan, "Progress of solar energy in Rajasthan," 2023, https://energy.rajasthan.gov.in/content/raj/energydepartment/rrecl/en/projects/completed.html.

[4] K. Kanwar and J. Vajpai, "MATLAB based comparative analysis of alternative PV models," in *Proceedings of International Conference on Intelligent Energy Management Technologies, Algorithms for Intelligent Systems*, Singapore, June 2021.

[5] G. M. Masters, *Renewable and Efficient Electric Power Systems*, John Wiley and Sons, Hoboken, NY, USA, 2004, https://onlinelibrary.wiley.com/doi/book/10.1002/0471668826.

[6] M. K. Fuentes, "Thermal model of residential photovoltaic arrays," in *Proceedings of 17th IEEE PV Specialists Conference*, pp. 1341–1346, Orlando, FL, USA, July 1984.

[7] T. Schott, "Operation temperatures of PV modules: a theoretical and experimental approach," in *Proceedings of 6th E.C. Photovoltaic Solar Energy Conference*, pp. 392–396, London, UK, August 1985.

[8] A. D. Jones and C. P. Underwood, "A thermal model for photovoltaic systems," *Solar Energy*, vol. 70, no. 4, pp. 349–359, 2001.

[9] W. Knaup, "Thermal description of photovoltaic panels," in *Proceedings of 11th E.C. Photovoltaic Solar Energy Conference*, pp. 1344–1347, Montreux, Switzerland, June 1992.

[10] M. Mattei, G. Notton, C. Cristofari, M. Muselli, and P. Poggi, "Calculation of the polycrystalline PV module temperature using a simple method of energy balance," *Renewable Energy*, vol. 31, no. 4, pp. 553–567, 2006.

[11] E. Skoplaki and J. A. Palyvos, "On the temperature dependence of photovoltaic module electrical performance: a review of efficiency/power correlations," *Solar Energy*, vol. 83, no. 5, pp. 614–624, 2009.

[12] S. Dubey, J. N. Sarvaiya, and B. Seshadri, "Temperature-dependent photovoltaic (PV) efficiency and its effect on PV production in the world – a review," *Energy Procedia*, vol. 33, pp. 311–321, 2013.

[13] E. Kaplani and S. Kaplanis, "Thermal modelling and experimental assessment of the dependence of PV module temperature on wind velocity and direction, module orientation and inclination," *Solar Energy*, vol. 107, pp. 443–460, 2014.

[14] S. Armstrong and W. G. Hurley, "A thermal model for photovoltaic panels under varying atmospheric conditions," *Applied Thermal Engineering*, vol. 30, no. 11-12, pp. 1488–1495, 2010.

[15] K. Kant, A. Shukla, A. Sharma, and P. H. Biwole, "Thermal response of poly-crystalline silicon photovoltaic panels: numerical simulation and experimental study," *Solar Energy*, vol. 134, pp. 147–155, 2016.

[16] M. Jaszczur, Q. Hassan, J. Teneta, E. Majewska, and M. Zych, "An analysis of temperature distribution in solar photovoltaic panel under various environmental conditions," in *Proceedings of the 11th International Conference on Computational Heat, Mass and Momentum Transfer (ICCHMT-2018)*, Cracow, Poland, June 2018.

[17] G. Notton, C. Cristofari, M. Mattei, and P. Poggi, "Modelling of a double-glass photovoltaic module using finite differences," *Applied Thermal Engineering*, vol. 25, no. 17–18, pp. 2854–2877, 2005.

[18] H. F. Tsai and H. L. Tsai, "Implementation and verification of integrated thermal and electrical models for commercial PV modules," *Solar Energy*, vol. 86, no. 1, pp. 654–665, 2012.

[19] C. A. Belhadj, A. M. Ba-Abbad, and R. Ben-Mansour, "An integrated thermal and electrical model for PV panel performance," in *Proceedings of 15th International Multi-Conference Systems, Signals & Devices*, pp. 769–772, July 2018, https://ieeexplore.ieee.org/document/8570608.

[20] K. Yaman and G. Arslan, "A detailed mathematical model and experimental validation for coupled thermal and electrical performance of a photovoltaic (PV) module," *Applied Thermal Engineering*, vol. 195, pp. 117224–117318, 2021.

[21] D. L. King, W. E. Boyson, and J. A. Kratochvil, *Photovoltaic Array Performance Model*, Citeseer, Princeton, NY, USA, 2004.

[22] J. A. Duffie and W. A. Beckman, *Solar Engineering of Thermal Processes*, John Wiley and Sons, Hoboken, NY, USA, 4th edition, 2013, https://www.wiley.com/en-in/Solar+Engineering+of+Thermal+Processes,+4th+Edition-p-9780470873663

[23] S. P. Aly, S. Ahzi, N. Barth, and A. Abdallah, "Using energy balance method to study the thermal behavior of PV panels under time-varying field conditions," *Energy Conversion and Management*, vol. 175, pp. 246–262, 2018.

[24] P. Bevilacqua, S. Perrella, R. Bruno, and N. Arcuri, "An accurate thermal model for the PV electric generation prediction: long-term validation in different climatic conditions," *Renewable Energy*, vol. 163, pp. 1092–1112, 2021.

[25] F. Nicoletti, M. A. Cucumo, V. Ferraro, D. Kaliakatsos, and A. Gigliotti, "A thermal model to estimate PV electrical power and temperature profile along panel thickness," *Energies*, vol. 15, no. 20, pp. 7577–7617, 2022.

[26] S. Khanam, M. Meraj, M. Azhar et al., "Comparative performance analysis of photovoltaic modules of different materials for four different climatic zone of India," *Urban Climate*, vol. 39, Article ID 100957, pp. 1–12, 2021.

[27] H. K. Khyani, J. Vajpai, and R. Karwa, "Effective cooling strategy for solar PV panels for the climatic conditions of Jodhpur," in *Proceedings of 36th National Conference on Future Electricity Systems: Challenges and Current Trends (NCEFES-2021)*, pp. 82–91, Noida, India, June 2021.

[28] K. Nishioka, K. Miyamura, Y. Ota, M. Akitomi, Y. Chiba, and A. Masuda, "Accurate measurement and estimation of solar cell temperature in photovoltaic module operating in real environmental conditions," *Japanese Journal of Applied Physics*, vol. 57, 2018.

[29] choosegreensolar, "Solar panel construction," 2020, https://choosegreensolar.com/solar-panel-construction/.

[30] K. Burrows and V. Fthenakis, "Glass needs for a growing photovoltaics industry," *Solar Energy Materials and Solar Cells*, vol. 132, pp. 455–459, 2015.

[31] R. Karwa, *Heat and Mass Transfer*, Springer Science, Singapore, 2020.

[32] S. Jiang, K. Wang, H. Zhang, Y. Ding, and Q. Yu, "Encapsulation of PV modules using ethylene vinyl acetate

copolymer as the encapsulant," *Macromolecular Reaction Engineering*, vol. 9, no. 5, pp. 522–529, 2015, https://onlinelibrary.wiley.com/doi/abs/10.1002/mren.201400065.

[33] R. Nasrin, N. A. Rahim, H. Fayaz, and M. Hasanuzzaman, "Water/MWCNT nanofluid based cooling system of PVT: experimental and numerical research," *Renewable Energy*, vol. 121, pp. 286–300, 2018.

[34] M. Hammami, S. Torretti, F. Grimaccia, and G. Grandi, "Thermal and performance analysis of a photovoltaic panel with an integrated energy storage system," *Applied Sciences*, vol. 7, no. 11, pp. 1–15, 2017.

[35] ASHRAE Standard, *Methods of Testing to Determine the Thermal Performance of Solar Collectors*, American Society of Heating, Refrigerating and Air-Conditioning Engineers, New York, NY, USA, 1977.

[36] I. Santiago, D. Trillo-Montero, I. M. Moreno-Garcia, V. Pallarés-López, and J. J. Luna-Rodríguez, "Modeling of photovoltaic cell temperature losses: a review and a practice case in south Spain," *Renewable and Sustainable Energy Reviews*, vol. 90, pp. 70–89, 2018.

[37] W. C. Swinbank, "Long-wave radiation from clear skies," *Quarterly Journal of the Royal Meteorological Society*, vol. 89, no. 381, pp. 339–348, 1963.

[38] W. H. McAdams, *Heat Transmission*, McGraw-Hill, New York, NY, USA, 2nd edition, 1954.

[39] D. L. Evans and L. W. Florschuetz, "Cost studies on terrestrial photovoltaic power systems with sunlight concentration," *Solar Energy*, vol. 19, no. 3, pp. 255–262, 1977.

[40] mynasadata, "My NASA data," 2023, https://mynasadata.larc.nasa.gov/.

[41] R. Karwa and G. Chitoshiya, "Performance study of solar air heater having V-down discrete ribs on absorber plate," *Energy*, vol. 55, pp. 939–955, 2013.

[42] S. J. Kline and F. A. McClintock, "Describing uncertainties in single sample experiments," *Mechanical Engineering*, vol. 75, pp. 3–8, 1953.

[43] R. Karwa, N. Karwa, R. Misra, and P. C. Agarwal, "Effect of flow maldistribution on thermal performance of a solar air heater array with subcollectors in parallel," *Energy*, vol. 32, no. 7, pp. 1260–1270, 2007.

[44] N. A. S. Elminshawy, A. Osama, N. Naeim, O. Elbaksawi, and G. M. Tina, "Thermal regulation of partially floating photovoltaics for enhanced electricity production: a modeling and experimental analysis," *Sustainable Energy Technologies and Assessments*, vol. 53, Article ID 102582, 2022.